

IMPACT OF MANUFACTURING VARIABILITY AND NON-AXISYMMETRY ON HIGH-PRESSURE COMPRESSOR STAGE PERFORMANCE

Alexander Lange, Matthias Voigt, Konrad Vogeler
Technische Universität Dresden
Institute of Fluid Mechanics
D-01062 Dresden, Germany
Email: alexander.lange@tu-dresden.de

Henner Schropp, Erik Johann, Volker Gümmer
Rolls-Royce Deutschland Ltd & Co KG
Compressor Aerodynamics
D-15827 Blankenfelde-Mahlow, Dahlewitz, Germany

ABSTRACT

This paper introduces an approach for considering manufacturing variability leading to a non-axisymmetric blading in CFD simulation of a high-pressure compressor stage.

A set of 150 rotor blades from a high-pressure compressor stage was 3D scanned to obtain the manufacturing variability. The obtained point clouds were parameterized using a parametric blade model, which uses typical profile parameters for translating the geometric variability into a numerical model. Probabilistic simulation methods allow for generation of a sampled set of blades that statistically corresponds to the measured one. This technique was applied to generate 4000 sampled blades to investigate the influence of a non-axisymmetric blading. It was found that the aerodynamic performance is considerably influenced by a variation of passage cross section. Nevertheless, this influence decreases with an increasing number of independently sampled blades and thus independently shaped passage cross sections. Due to a more accurate consideration of the geometric variability, the presented methodology allows for a more realistic performance analysis of an HPC stage.

NOMENCLATURE

c_p	pressure coefficient
j, k	index in spanwise, streamwise direction
\dot{m}	mass flow
M_{rel}	relative Mach number
N	number
p	static pressure, index of passage
p_t	total pressure
s	spanwise coordinate: $s = r / (r_{casing} - r_{hub})$

t	thickness
w	camber
γ_P	stagnation pressure loss coefficient
β_{out}	stage outlet angle
$\Delta\beta$	blade turning
η	isentropic efficiency
λ	ratio of statistical parameters
$\tilde{\lambda}$	approximated ratio of statistical parameters
μ	mean value
Π	total pressure ratio
σ	standard deviation

Abbreviations

CFD	computational fluid dynamics
HPC	high-pressure compressor
LE, TE	leading edge, trailing edge
MCS	Monte-Carlo simulation
PCA	principal component analysis
pdf	probability density function
SoP	Statistics on Passage

1 INTRODUCTION

The influence of manufacturing variability on the performance of gas turbine blades has been subject to various investigations in recent years. GARZON and DARMOFAL [1] introduced a methodology for considering real geometry in CFD simulation through the principal component analysis (PCA) of coordinate-measuring machine (CMM) based surface measurements of rotor blades. This approach allowed for a reduction of the three-dimensional deviations to few modes and corresponding amplitudes. This mathematical information was used to perform a

probabilistic CFD simulation with 2D flow solver MISES to obtain results such as loss coefficient and blade turning including their statistical behavior. LANGE et al. [2] introduced a model especially designed for compressor blades, that allowed the parametrization of real blades through design like parameters. The same authors applied this model to a set of 3D scanned compressor blades of a high-pressure compressor (HPC) stage to investigate the impact of the geometric variability on the performance of the HPC stage [3]. This probabilistic 3D CFD simulation determined the scatter range of global result variables (e.g. efficiency) including their sensitivity to the geometric parameters.

Both previous investigations assumed an axisymmetric blading with identical blades in the circumferential direction and thus identical blade passages for the entire rotor. In real life each blade and each passage will be different. This paper addresses this problem of non-axisymmetric blading. By considering up to eight individual rotor blade geometries in one row it was possible to account for the variation of the passage geometry. See Fig. 1 for the 8 passages model. Consequently, the influ-

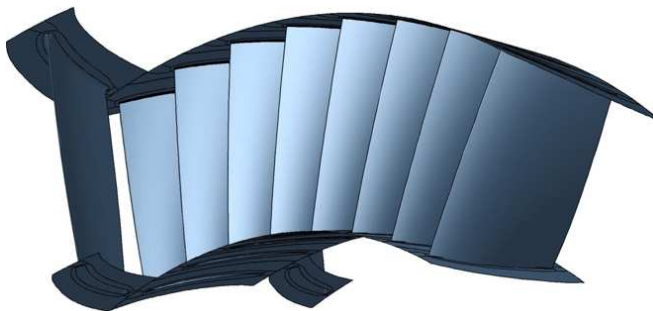


Figure 1: 1.5 HPC stage model with eight individual rotor passages.

ence of the changed flow conditions in one passage depending on the flow conditions in the other passages can be investigated. Furthermore this approach allows a description of the integral behavior of independently shaped passages and thus a quantification of the amplification or reduction of the scatter range compared to a conventional single passage calculation. In this context it becomes apparent that for non-axisymmetric blading the parameters of main influence are likely to be different to those of axisymmetric blading. Altogether, the present investigation provides a more generalized approach compared to the work of LANGE et al. [3]. Due to considering more variability features it allows for the identification of non-axisymmetric flow phenomena and finally leads to a more realistic performance analysis of the HPC stage.

2 DETERMINISTIC MODEL

The developed process chain is applied to a 3D CFD model of a stator-rotor-stator configuration taken from one of the mid stages of a multi stage high pressure compressor. The mesh generation was done with Numeca's AutoGrid [4] allowing 300k nodes per row and thus 900k nodes in total. By default a single passage model is obtained. The multi-passage models were created in Numeca's preprocessor IGG by duplication of the rotor blocks and adjusting the periodic boundary conditions with respect to the number of meshed passages. Eventually four different models were constructed: the conventional single passage model and three multi-passage models with 2, 4 and 8 rotor passages. At the inlet radial profiles of total pressure, total temperature and the air angles were prescribed. At the exit a static pressure profile was set as boundary condition. The flow solution was calculated with Numeca's FINE/Turbo 8.5-1 [5]. Convergence was reached quickly within 300 iterations using a convenient initial solution. The calculation time ranged from approximately 15 min for the single passage model up to approximately 45 min for the 8 passages model on 4 cores of an Intel core i7 CPU.

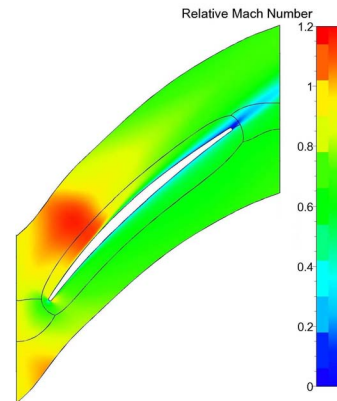


Figure 2: Relative Mach number at 75% span.

The deterministic solution will not be discussed in detail, since the probabilistic approach focusses on the scatter of results caused by the scatter of input parameters. One feature has a major influence on the result variables; the extension and the magnitude of the supersonic region caused by the suction peak, see Fig. 2. Its impact on the scatter of the results will be discussed in section 5.

3 MODELLING OF GEOMETRIC VARIABILITY

The geometric variability of the rotor geometry is based on 150 HPC blades. They were 3D scanned using a 3D digitizer. The registration of the scan was done using the contact surfaces in the

blade root. The parametric compressor blade model of LANGE et al. [2] was used to parameterize the geometric variation of the surface of the blades, see Tab. 1 for the set of geometric parameters.

Table 1: Geometric parameters.

symbol	parameter
ax, tan	axial and tangential position of section outline at leading edge
λ	stagger angle
c	chord length
t_{LE}, t_{TE}	leading edge and trailing edge thickness
$pos_{t_{LE}}, pos_{t_{TE}}$	assigned position on chord
t_{max}, w_{max}	maximum thickness and camber of profile
$pos_{t_{max}}, pos_{w_{max}}$	assigned position on chord
β_{LE}, β_{TE}	angle of camber line at leading edge and trailing edge
t_f, s_f	thickness and height of the fillet

These parameters resemble the basic design parameters that the aerodynamics engineer is more familiar with than a set of eigenvectors originating from a PCA. The choice of parameters therefore makes it easier to exploit the results. The parameters are calculated for the set of scanned blades and for the reference geometry (e.g. CAD geometry) to quantify the differences between real geometry and manufacturing intention. These differences then are added to the hot geometry to obtain a CFD model of the real blade. This approach implies the assumption that the geometric variability is comparatively small and thus does not affect the cold-hot transformation. The correlation of the parameters over blade height allows a reduction of the parameters by averaging over span. Consequently, the 3D deviations are described by an averaged delta parameter vector. LANGE et al. [3] carried out a study concerning the required numbers of radial averaged zones to correctly rebuild scanned blades. They showed that one spanwise averaged zone may be sufficient to cover over 93% of scatter range by means of integral aerodynamic results. This strongly depends on the correlation of the parameters over blade height and thus principally on the manufacturing technology. Based on the observations made in [3], the number of averaged zones was set to two for this investigation since the manufacturing background is known to be similar. In contrast to one zone, two zones allow reproduction of the correct orientation of the blades and thus to model the variation of passage cross section in the radial direction. For illustration purposes a sampled 2 passages model is compared to the baseline geometry in Fig. 3. To summarize, the whole process chain contains the following steps:

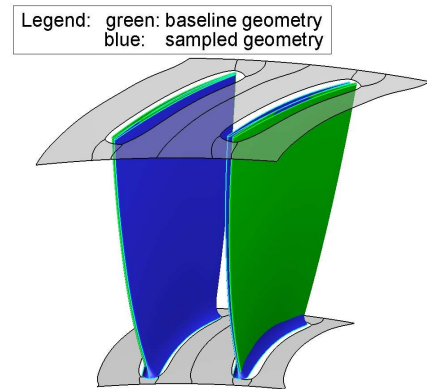


Figure 3: Geometry of a sampled 2 passages model with reasonable change in passage cross section.

- i) 3D scan and registration in blade root
- ii) parameter identification on sections of constant span
- iii) calculation of delta parameter vector (difference of scanned blade to cold reference geometry)
- iv) statistical analysis of delta parameter matrix of entire population
- v) setup of probabilistic model
- vi) generation of surface meshes of the rotor blades by adding the sampled delta parameter vector to the hot reference geometry
- vii) mesh morphing of the rotor blade passages to achieve the final CFD model

4 PROBABILISTIC MODEL

The probabilistic simulation was performed using ProSi (Probabilistic Simulation) — a tool that was developed at TU Dresden, Institute of Fluid Mechanics [6].

The probabilistic model corresponds to that of LANGE et al. [3], but the number of blade passages was increased to 8. With 14 geometric parameters per blade section and two averaging zones over the blade height plus two fillet parameters a total of 30 parameters were considered per blade, see Tab. 1. This results in 30, 60, 120 and 240 Parameters for the 1, 2, 4 and 8 passage models, respectively. This large number of parameters requires a large number of simulations. In this case the Monte-Carlo method was considered the best approach since the required number of shots (evaluations of deterministic model) hardly increases with the number of parameters, as described by HALDAR and MAHADEVAN [7]. However, a comparatively high number of 500 shots was used for each of the four probabilistic simulations. The total computational time was approximately 40 days. This time could be reduced significantly by distributing the deterministic runs on several machines.

The most suitable probabilistic density function (pdf) of each parameter was based on the outcome of an Anderson–Darling goodness–of–fit test. The minimal AD–criteria prescribes the pdf that best approximates to each determined distribution. The set of pdfs that were tested included Gaussian, Weibull, lognormal, triangular and uniform distributions. Gaussian, lognormal and Weibull were found to be the best approximation function 10, 13 and 7 times, respectively. The dependencies of the identified geometric parameters were quantified using a matrix of Spearman rank correlation coefficients, see SPEARMAN [8]. This matrix assures the reconstruction of realistic blades. It is prescribed when arranging the random numbers of all parameters by restricted pairing, as described by DANDEKAR et al. [9]. Thus a 30×30 matrix describing the correlations of the scanned blade set is used for each rotor blade. The individual blades — in contrast — are modelled independently. The entire correlation matrix contains 240×240 variables resulting from 8 blades with 30×30 variables each.

5 RESULTS

Within the probabilistic investigation 500 deterministic simulations for each of the four models were performed. Figure 4 illustrates the benefit of a probability based analysis. It shows the static pressure on the washed surfaces of one selected realization and its variations due to individual blade geometries. Although, 3D CFD allows this detailed look inside the flow field, it is not possible to investigate all deterministic simulations of a probabilistic simulation. One option is to derive less dimensional re-

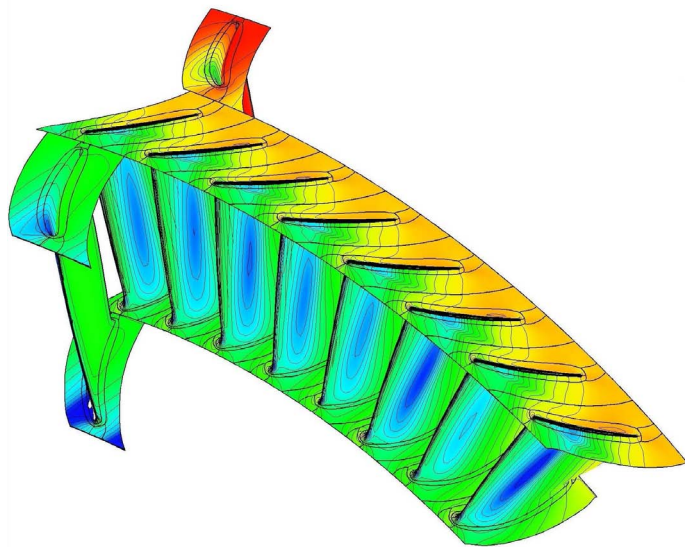


Figure 4: 3D Pressure field of one realization.

sults from the flow solution. Integral values (e.g. efficiency) are especially advantageous for further postprocessing. In addition a statistics based flow analysis — Statistics on Passage (SoP) — is introduced in section 5.2. With SoP 3D results of the entire probabilistic simulation can be analyzed simultaneously. The method provides statistical values and sensitivities of flow solution quantities to input parameters and leads to a better understanding of the flow physics.

5.1 Integral results

The histogram of isentropic efficiency gives a quick overview of the integral behavior of the stage, see Fig. 5. In addition an Ant–Hill plot of isentropic efficiency vs. mass averaged total pressure loss y_P of the rotor row,

$$y_P = \frac{1}{\dot{m}} \sum_j \frac{\dot{m}_j (p_{t \text{ outlet},sl} - p_{t \text{ inlet},j})}{p_{t \text{ inlet},j} - p_{\text{inlet},j}}, \quad (1)$$

allows the correlation between these two result values to be estimated for all performed simulations, see Fig. 6. Furthermore, unusual events may be identified since all calculated shots are shown.

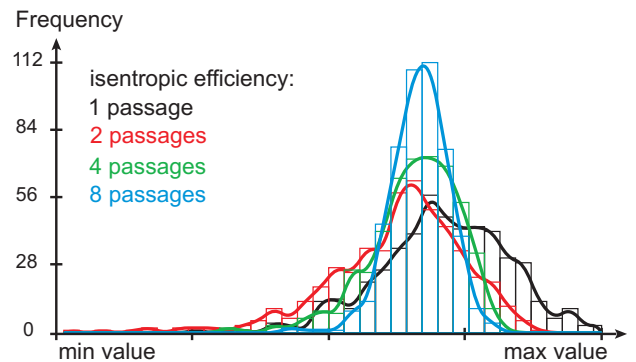


Figure 5: Histogram of isentropic efficiency for 1, 2, 4 and 8 passages calculation.

Both plots show that the scatter range of the results decreases and the density around the mean value increases with increasing number of passages. Accordingly, the scatter clouds in Fig. 6 concentrate for higher number of passages in the center nested in clouds of the remaining simulations. This occurs due to the statistical properties of the individual blades, that were modelled independently. The probability for blade 2 being a "good" one (in terms of loss coefficient) does not depend on the properties of blade 1 (which could be thicker and therefore cause higher losses) and vice versa. Ultimately, there will be a mixture of

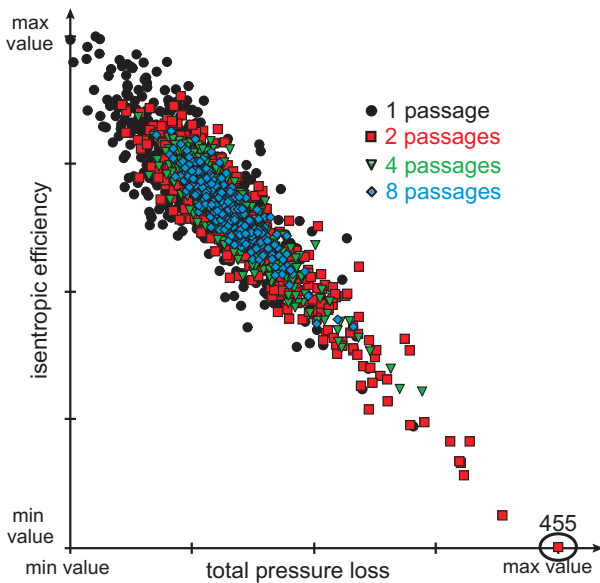


Figure 6: Ant-Hill plot of isentropic efficiency vs. total pressure loss for 1, 2, 4 and 8 passages calculation.

”good” and ”bad” blades and it is rather unlikely that an 8 passage model consists of ”good” or ”bad” blades only. This shows, that the classical approach of an axisymmetric single passage calculation is a very rough simplification of turbomachinery flow.

In contrast to this general tendency an increased scatter range is obtained for some result quantities of the 2 passages calculation, see Fig. 5 and 6. The reason for this increase is the change of passage cross section due to changing blade positions. The single passage calculation cannot account for this phenomenon and thus shows less scatter. The multi-passage models, in contrast, have an implicitly increased degree of freedom. They are able to describe different flow conditions in each passage caused by interactions in the circumferential direction. Consequently they allow for a more accurate investigation of real geometry flow simulation, see Fig. 4 for a qualitative overview.

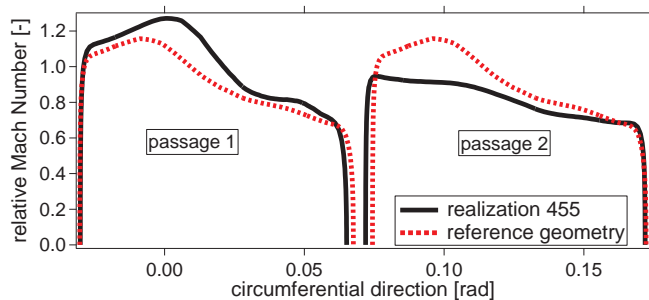


Figure 7: Comparison of relative Mach number vs. circumferential coordinate at 75% span and 30% chord.

The altered passage flow is quantified for realization 455, labeled in Fig. 6. This 2 passage configuration is characterized by the lowest isentropic efficiency of all 2000 realizations. One explanation for the low efficiency may be found in the high level of circumferential variation and thus different velocities in the individual passages. The selected realization shows a significantly higher peak Mach number in passage 1 ($M_{rel} \approx 1.25$) than in passage 2 ($M_{rel} \approx 0.98$). The peak Mach number of the reference geometry is $M_{rel} \approx 1.15$. Figure 7 shows the variation of relative Mach number with circumferential direction along a line at 30% axial chord on the 75% span surface (line indicated in Fig. 8). In addition, the pressure field is analyzed for the same span surface. It confirms the results of the relative Mach number plot and indicates the uneven load share between the two passages, see Fig. 8. This results in a significantly reduced static pressure at the acceleration area in passage 1 (center) that leads to higher Mach numbers. Consequently, in passage 2 (upper and lower half passage) the static pressure shows lower gradients and the Mach number distribution remains almost uniform.

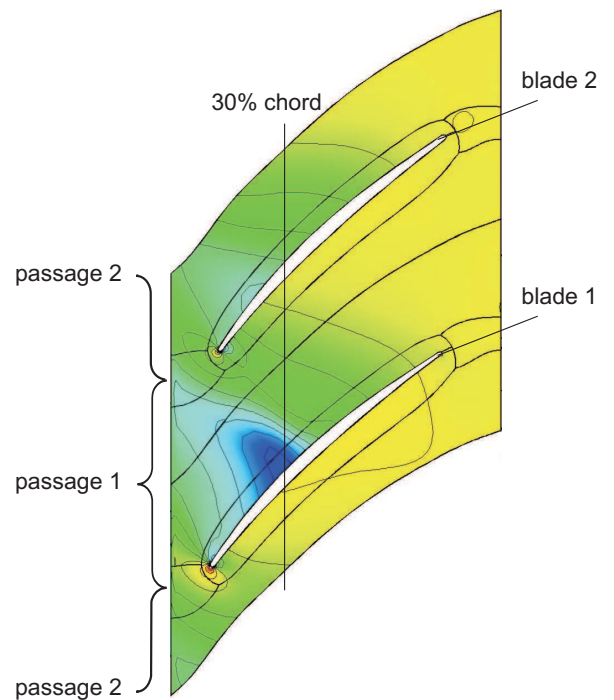


Figure 8: Static pressure of rotor of realization 455 at 75% span.

Another suitable non-dimensional variable is the pressure coefficient

$$c_{p,k} = \frac{p_k}{p_{inlet} - p_{inlet}} \quad (2)$$

It describes the static pressure at the surface of the blades and can be used to indicate a change in the Mach number distribution. By evaluating all realizations, a vector with 500 values of c_p is obtained for each node k . A statistical description of the variations is done by mean value and standard deviation. Figure 9 shows a comparison between the pressure coefficients of the single passage and the 2 passages calculation. The mean value of the pressure coefficient is plotted as a solid line, the standard deviation is indicated by error bars. Obviously the 2 passages calculation implies larger variations of the static pressure — especially in the supersonic region on the suction side. Due to the changed passage cross section, the variation of the position and the magnitude of the maximum relative Mach number profile is higher. This explains the considerably changed relative Mach number profile of realization 455 shown in Fig. 7. While the standard deviation shows significant differences, the mean value distributions are more similar. Only the suction side curve is slightly smoother in the case of the 2 passages solution.

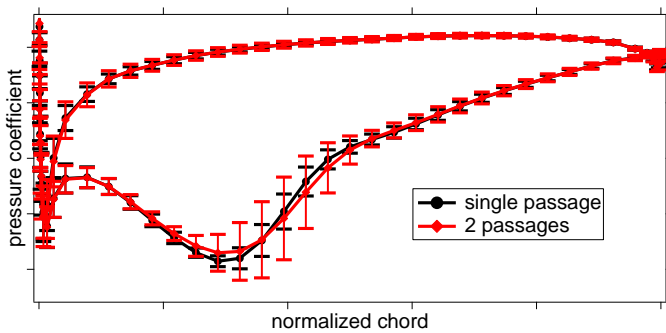


Figure 9: Comparison of pressure coefficient between single passage and 2 passages model at 75% span.

5.2 Statistics on Passage

A statistical approach to quantify the variation of a 3D result quantity on a CFD grid is provided by a novel postprocessing methodology — Statistics on Passage (SoP). The development of SoP was inspired by previously presented statistical postprocessing tools for finite element structures, e. g. Statistics on Structure (SoS) by BAYER and ROOS [10]. SoP facilitates the postprocessing of a probabilistic CFD simulation and leads to increased understanding of the dependencies of the flow. It describes the variation of the 3D flow field quantity (e.g. the static pressure) statistically by analyzing all nodes of all realizations.

In the present investigation SoP is applied to quantify the higher variations of the static pressure in the supersonic region of the 2 passages model and to estimate the influenced domain. For this purpose the standard deviation of the static pressure field of the single passage model is compared to that of the 2 passages model, see Fig. 10.

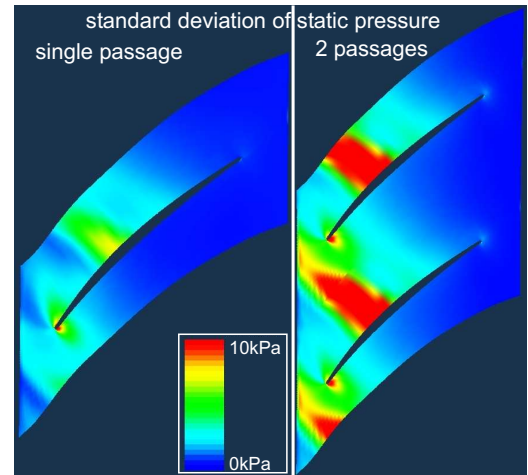


Figure 10: Std. deviation of static pressure field at 75% span.

In accordance with Fig. 9, the higher standard deviation of the 2 passages model — especially around 30% chord on the suction side — indicates the significant influence of the variable passage cross section on the suction peak of the static pressure. While standard deviation of the single passage model hardly touches the value of 10 kPa, the 2 passages model exceeds it clearly. In contrast to this result, both models show nearly the same behavior close to the leading edge. Here, the standard deviation of the static pressure is of the same order of magnitude in both cases. Apparently the geometry variations at the leading edge induce disturbances of locally limited influence.

For each node of the CFD mesh the correlation of any flow quantity with any probabilistic parameter can be calculated. The contour plots in Fig. 11 show the correlation of the static pressure with maximum camber for the single passage model on the left and for each of the two blades of the 2 passages model on the right.

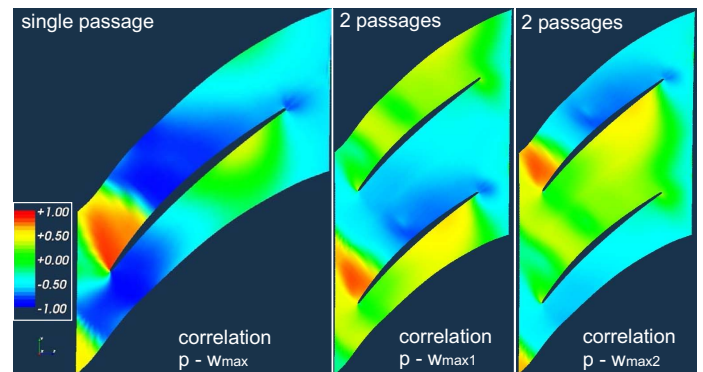


Figure 11: Correlation between static pressure field and maximum camber at 75% span.

In both cases the parameter maximum camber has a major effect on the pressure field. In the single passage model an increased maximum camber leads to higher static pressure values upstream and lower values downstream of a position at approximately 30% chord. The variation of the static pressure propagates through the periodic boundary and can thus also be detected on the pressure side. In case of the 2 passages model the maximum camber predominantly influences the variations at the suction side of the particular blade. Since the second blade is assumed to be statistically independent, the induced variations reduce significantly expressed by correlation coefficients close to zero.

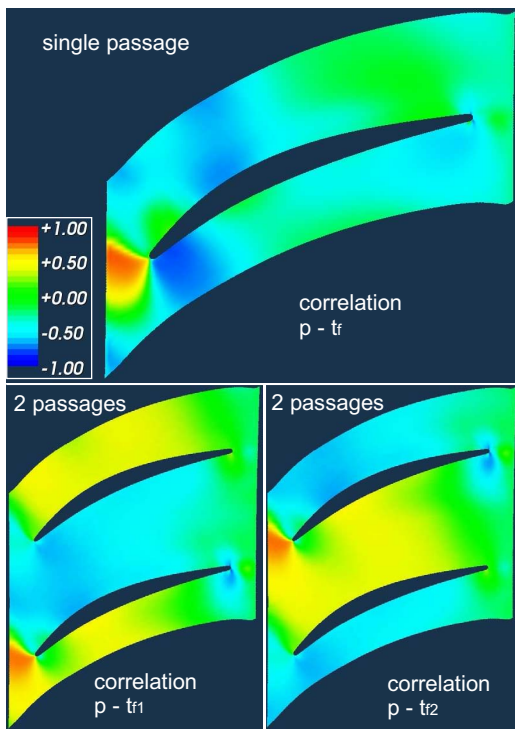


Figure 12: Correlation between static pressure field and fillet thickness at 5% span.

Another parameter of major influence on the static pressure field close to the hub is the thickness of the fillet. Both models indicate a positive correlation of the static pressure around the stagnation point at the leading edge with the thickness of the fillet, see Fig. 12. This is expected since a thicker blade increases the deceleration area and leads to higher static pressures. The main difference between the two models can be found further downstream. In the single passage model the correlation plot indicates a tendency to lower static pressures and higher velocities, which may result from a smaller cross sectional area of the passage. The opposite is observed for the 2 passages model, where the acceleration region is limited to the passage adjacent to the suc-

tion side of the corresponding blade (e.g. passage 1 for blade 1 according to notation of Fig. 8). The other passage at the pressure side, however, shows an inverse behavior with higher static pressure and lower velocity.

5.3 Extrapolation to 360° Rotor (full annulus)

This section addresses the statistical evaluation of the result value distributions of each of the four models. The aim is to derive a law for the statistical behavior of the full annulus rotor with all blades considered as individual and independently sampled. It is assumed that all result values are normally distributed and can be described by mean value and standard deviation. To indicate the reliability of these estimates a confidence interval with 95% confidence level is calculated [11]. It turned out to be advantageous to use the single passage simulation as reference when investigating the dependencies of the statistical estimates on the number of passages. Consequently, the ratio of standard deviations

$$\lambda_{\sigma} = \frac{\sigma_p}{\sigma_1} \quad (3)$$

and the difference of the mean values (mean value shift) normalized by the standard deviation of the single passage model

$$\lambda_{\mu} = \frac{\mu_p - \mu_1}{\sigma_1} \quad (4)$$

are analyzed.

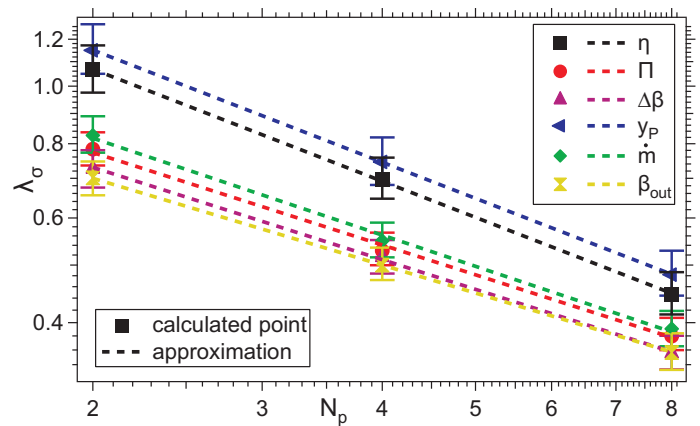


Figure 13: Approximation of standard deviation ratio.

For the standard deviation a linear characteristic of λ_{σ} over the number of passages was observed when using a log-log system.¹

¹The authors found similar tendencies in other non-axisymmetric investigations.

For the case considered, the confidence interval of $\Delta\lambda_\sigma/\lambda_\sigma$ ranges between 12% and 19% of the corresponding value, see Fig. 13. This indicates a reliable solution, since the change of λ_σ over N_p is significantly higher. Based on this phenomenon a linear function

$$\ln(\tilde{\lambda}_\sigma) = A_0 + A_1 \ln(N_p) \quad (5)$$

is fitted to approximate the points. This empirical law allows estimation of the standard deviation of the 360° rotor

$$\sigma_{360^\circ} = \sigma_1 e^{A_0 + A_1 \ln(N_{p,360^\circ})} \quad (6)$$

with independently arranged blades for all passages. As Fig. 13 shows, the curves converge for higher number of passages. The values for the extrapolated 360° model are similar for the analyzed result variables within a range of $\lambda_\sigma(N_{p,360^\circ}) = [0.126 \dots 0.137]$. This means that the scatter of all these quantities is expected to reduce to about 13% compared to the scatter of the single passage model.

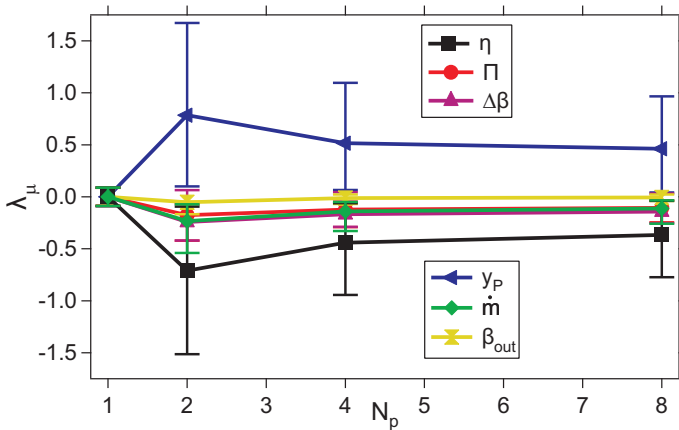


Figure 14: Mean value shift.

Figure 14 shows the mean value shift plotted vs. the number of passages. Unfortunately, no corresponding empirical law could be derived. Only a tendency of stabilization for higher numbers of passages is observed. The 2 passages model has the highest probability for combining extreme blades, leading to a greater variation in passage cross section. As a result, the mean value shift λ_μ and the corresponding confidence interval for the 2 passages model shows larger values than for the remaining models. The efficiency and loss coefficient show a higher sensitivity to a variation of passage cross section. Their curves are characterized by large confidence intervals. These conclusions lead to

the interpretation, that the prediction of the mean value shift is difficult — especially for the efficiency and the loss coefficient. Nevertheless, the tendencies of the shift are as expected. A reduction in efficiency correlates with a increased loss coefficient. At the same time, the remaining result values in Fig. 14 show the expected slight decrease.

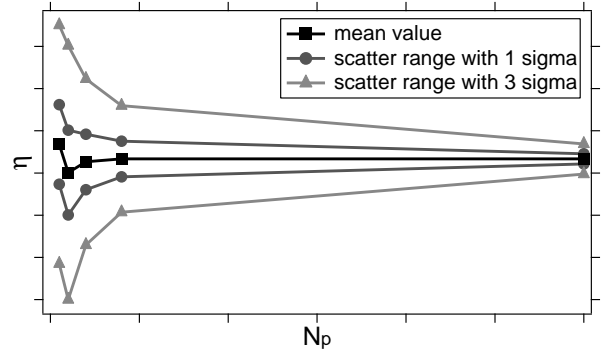


Figure 15: Scatter range extrapolation for isentropic efficiency.

The calculation of the scatter range of the 360° rotor is prescribed by an extrapolation of standard deviation (Eq. 3 and 6) and mean value. As explained before, no empirical law could be derived for the mean value shift. Due to this lack of knowledge, the mean value shift of the full annulus rotor model is assumed to be equal the result of the 8 passages calculation:

$$\lambda_\mu(N_{p,360^\circ}) \approx \lambda_\mu(N_p = 8). \quad (7)$$

Together with Eq. 4 the extrapolation rule is completely defined. With this set of equations the scatter range for an arbitrary number of independently sampled blades can be approximated. Figure 15 shows this approximation for the isentropic efficiency at the 1 sigma and 3 sigma level.

Table 2: Scatter range of isentropic efficiency for three passage numbers with reference to single passage scatter range.

scatter range	1 passage	2 passages	360°
$\sigma(\eta_p) / \sigma(\eta_1)$	1	1.06	0.13
$[\mu(\eta_p) - \mu(\eta_1)] / \sigma(\eta_1)$	0	-0.71	-0.37
$\Delta\eta / \sigma(\eta_1)$ (1 sigma)	-1...1	-1.78...0.35	-0.49...-0.24
$\Delta\eta / \sigma(\eta_1)$ (3 sigma)	-3...3	-3.90...2.48	-0.75...0.01

Based on the presented approach, a worst-case estimate may be added, see Tab. 2. Obviously, the three models of major interest

are the single passage, the 2 passages and the 360° extrapolation. The biggest scatter range is observed for the 2 passages model. Due to a shift of the mean value, the highest efficiency is likely to occur for the single passage model, while the lowest value is found for the 2 passages model. Finally the 360° extrapolation shows a significant reduction in scatter.

6 CONCLUSIONS

This paper introduced a method for considering manufacturing variability leading to a non-axisymmetric blading in a CFD simulation. Geometric variability was quantified from optical measurements of a set of 150 HPC rotor blades that were parameterized by a parametric blade model that uses typical profile parameters. The non-axisymmetric blading was set up using four different models containing from 1 up to 8 meshed passages that all consist of individual blade geometries. Probabilistic sampling methods were used to create these different geometries. The sampled blades of each passage correspond to the measured set of blades statistically. However, each blade was modelled independently of its neighbors.

The presented approach gives access to the simulation of the changed flow conditions of non-axisymmetric blading. It allows investigating of the influence of distortions induced by one blade on the flow conditions in adjacent passages. It was shown that the aerodynamic performance is considerably influenced by a change in passage cross section. This leads to a change of the integral behavior of the HPC stage and consequently to a change of the scatter range of representative results. Based on these conclusions an empirical law was derived that quantifies the statistical properties with respect to the number of passages and allows for extrapolation to the full annulus rotor properties.

The obtained results principally indicate an amplification up to 106% (for the 2 passages model) and reduction to 13% (extrapolated for the full annulus rotor model) of the scatter range of isentropic efficiency compared to the values of a single passage calculation. As well as the change of standard deviation, a shift of the mean value was also observed that decreases with increasing number of passages. This result strongly relies on the probabilistic model referring to independently sampled blades. It represents the clear opposite to the conventional single passage approach that assumes identical blades in the circumferential direction. Consequently, both approaches represent extreme solutions. They allow the engineer to set the limits for the application of interest with probably minor dependencies between the individual blades of the entire rotor.

Altogether, the presented investigation provides a more generalized approach than the standard single passage calculation. By considering more variability features it allows identification of the non-axisymmetric flow phenomena and finally leads to a more realistic performance analysis of the HPC stage.

ACKNOWLEDGMENT

The authors would like to thank Rolls–Royce Deutschland Ltd & Co KG for encouraging and approving the publication of this work. The project is funded by Rolls–Royce Deutschland Ltd & Co KG and the Bundesministerium für Wirtschaft und Technologie under the contract FNZ20T0609. Academic licenses of Numeca FINE/Turbo 8.5-1 were used.

REFERENCES

- [1] Garzon, V. E., and Darmofal, D. L., 2003. “Impact of geometric variability on axial compressor performance”. *ASME paper no. GT2003-38130*.
- [2] Lange, A., Vogeler, K., Gümmer, V., Schrapp, H., and Clemen, C., 2009. “Introduction of a parameter based compressor blade model for considering measured geometry uncertainties in numerical simulation”. *ASME paper no. GT2009-59937*.
- [3] Lange, A., Voigt, M., Vogeler, K., Schrapp, H., Johann, E., and Gümmer, V., 2010. “Probabilistic CFD simulation of a high pressure compressor stage taking manufacturing variability into account”. *ASME paper no. GT2010-22484*.
- [4] NUMECA, 2007, *User Manual AutoGrid v8*.
- [5] NUMECA, 2008, *User manual FINE/Turbo v8.5*.
- [6] Voigt, M., Bischoff, T., and Lang, G., 2008. *Prosi Manual*. TU Dresden, Institute of Fluid Mechanics, http://www.probabilistik.de/prosi_manual.pdf.
- [7] Haldar, A., and Mahadevan, S., 1999. *Probability, Reliability, and Statistical Methods in Engineering Design*. Wiley.
- [8] Spearman, C., 1904. “The proof and measurement of association between two things”. *The American Journal of Psychology*, **15**, pp. 72–101.
- [9] Dandekar, R. A., Cohen, M., and Kirkendall, N., 2001. “Applicability of Latin hypercube sampling technique to create multivariate synthetic microdata”. *Luxembourg: Eurostat in Proc. of ETKNTTS*, pp. 839–847.
- [10] Bayer, V., and Roos, D., 2006. “Non-parametric structural reliability analysis using random fields and robustness evaluation”. *Beiträge der Weimarer Optimierung- und Stochastiktage 3.0, Weimar, Germany*.
- [11] Bucher, C., 2009. *Computational Analysis of Randomness in Structural Mechanics*. CRC Press.